Earth and Planetary Science Letters 539 (2020) 116090

Contents lists available at ScienceDirect

Earth and Planetary Science Letters

www.elsevier.com/locate/epsl

Chemical evolution of the continental crust from a data-driven inversion of terrigenous sediment compositions

Matouš P. Ptáček [a], Nicolas Dauphas [a,*], Nicolas D. Greber [b]

[a] Origins Laboratory, Department of the Geophysical Sciences and Enrico Fermi Institute, The University of Chicago, 5734 South Ellis Avenue, Chicago IL 60637, USA
[b] Institut für Geologie, Universität Bern, 3012, Bern, Switzerland

ARTICLE INFO

Article history:
Received 13 March 2019
Received in revised form 27 December 2019
Accepted 9 January 2020
Available online 15 April 2020
Editor: R. Dasgupta

Keywords:
Archaean geochemistry
continental composition
crustal geotherm
plate tectonics

ABSTRACT

The nature of emerged continents through time is highly debated. Several studies relying on trace element data concluded that the Archaean crust was predominantly mafic, while Ti isotope systematics point to an Archaean crust that was predominantly felsic. Here, we resolve the inconsistency between these two approaches by applying a novel statistical method to a compilation of published elemental concentrations in terrigenous sediments (the OrTeS database). We use a filter based on the Local Outlier Factor to reject sediment samples that have been affected by alteration processes or mineral fractionation during transport. The nature of the emerged continents is calculated using an inverse mixing model based on a Markov Chain Monte Carlo algorithm. A procedure is presented to automatically select elemental ratios that are best suited for constraining the sediment provenance. We find that for all systems that accurately reconstruct the modern-day composition of the continents, a continuous >50% felsic contribution is required to explain the composition of fine-grained terrigenous sediments starting from 3.5 billion years ago. This finding is consistent with an early onset of plate tectonics. We estimate the geothermal gradient in the Archaean upper continental crust by tracking the reconstructed concentrations of the radiogenic heat-producing elements K, U, and Th through time. Radioactive heat production in the bulk continental crust was 50% higher in the Archaean compared to the present, resulting in a continental geothermal gradient that was about 40% higher.

1. Introduction

The operation of plate tectonics on the Earth today shapes many aspects of its habitability and long-term sustainability – controlling topography, climate feedbacks, and the supply of biochemically-important elements to the oceans. Establishing the time when plate tectonics started is important for understanding the conditions that allowed life to emerge and thrive, as well as constraining Earth's early geodynamics. Very diverse initiation ages for plate tectonics can be found in the literature (from 0.85 to >4.2 Ga; Hopkins et al., 2008; Korenaga, 2013; Tang et al., 2016; Greber et al., 2017; Greber and Dauphas, 2019; Brown and Johnson, 2018; Cawood et al., 2018; Rosas and Korenaga, 2018; Holder et al., 2019). One approach to constraining the beginnings of plate tectonics is to measure the composition of fine-grained terrigenous sedimentary rocks (primarily shales and diamictites) and thereby infer the nature of igneous rocks exposed to weathering on emerged continents (Tang et al., 2016; Greber et al., 2017; Greber and Dauphas, 2019). A limitation of this approach is that it cannot provide any constraint on the nature of submerged continents, which could have dominated in the Archaean (Flament et al., 2008; Korenaga et al., 2017; Bindeman et al., 2018).

Subduction processes and associated arc magmatism is conducive to the production of large areal extents of felsic rocks on continents (Arndt, 2013; Tang et al., 2016; Greber et al., 2017). In the Archaean, the argument has been made that felsic rocks known as TTGs (Tonalite-Trondhjemite-Granodiorite) could have been produced by melting of a thickened mafic oceanic crust (Smithies, 2000). In this model, extraction of TTG melts formed by melting of hydrated basaltic crust would leave behind a refractory residue. While some felsic rocks could undoubtedly be produced by this process, it is not clear whether these would be volumetrically important (Roman and Arndt, 2019). For example, in modern-day Iceland, felsic rocks represent only ~6-10% of exposed rocks. Hence, detecting a large contribution of felsic rocks to terrigenous sedimentary rocks may be indicative that subduction and possibly plate tectonics were operating.

Two types of terrigenous sediments have been used to infer the composition of the crust: diamictites and shales. Diamictites are the products of continental erosion by glaciers. Although they

* Corresponding author.
E-mail address: dauphas@uchicago.edu (N. Dauphas).

https://doi.org/10.1016/j.epsl.2020.116090
0012-821X/

provide a means of assessing the composition of the crust (*e.g.*, Gaschnig et al., 2016; Tang et al., 2016; Chen et al., 2019), they are scarce in the geological record. Shales are ubiquitous sedimentary rocks that were formed by the deposition of fine-grained marine sediments but they can suffer from chemical alteration as well as mineral fractionation caused by size or density sorting during weathering and transport.

In their seminal study, Taylor and McLennan (1985) demonstrated that several geochemical ratios in shales, including Th/Sc, La/Sc, and $\sum$LREE/$\sum$HREE, all display significant changes at around 3.0 to 2.5 Ga. Consistently, these ratios shift from (apparently) more mafic signatures in the Archaean to modern-like, felsic signatures in the post-Archaean. In the past several years, many geochemical ratios in fine-grained terrigenous sediments (*e.g.*, Cr/U, Cr/Zn, Nb/Ta, Ni/Co, Cu/Al_2O_3) have been brought to bear on the issue of the nature of the early emerged crust. These studies all agree that the early Archaean Earth was predominantly mafic, and transitioned to its modern felsic state at around 2.5 Ga (Large et al., 2018; Smit and Mezger, 2017; Sun, 2018; Tang et al., 2016; Chen et al., 2019). Meanwhile, other studies based on Ti isotopes and some geochemical ratios (Al/Ti, Zr/Ti, La/Sc, Th/Sc, Cr/Sc, Ni/Co) reached the opposite conclusion that the Archaean emerged continental crust was predominantly felsic since at least 3.5 Ga (Greber et al., 2017; Greber and Dauphas, 2019). This would support an early initiation of subduction and possibly plate tectonics. Mapping of Archaean terranes shows that they comprise 75% felsic rocks, 18% mafic rocks, and 7% ultramafic rocks (Condie, 1993). This suggests that either the geochemical proxies pointing to a predominantly mafic Archean continental crust were misinterpreted, or that these predominantly-felsic Archaean terranes are affected by a strong preservation bias.

The purpose of this study is to perform a data-driven quantitative re-analysis of published sedimentary geochemical compositions, employing modern statistical methods (supplementary file mmc1) to estimate the emerged crust composition as a function of time. Our methods aim to identify and eliminate biases that might have affected earlier studies. We then apply our compositional model to estimate the geothermal gradient within the early Archaean crust.

2. Methodology

Our approach is based on a three-endmember mixing model (Tang et al., 2016; Greber et al., 2017; Greber and Dauphas, 2019; Chen et al., 2019). We assume that most of the continental crust is sourced from mixtures of mafic, felsic, and ultramafic rocks (mainly in the form of komatiites until 2.5 Ga). We use igneous rock databases to calculate the compositions of these three endmembers. Then, we use measured elemental ratios in sediments to calculate what endmember mixtures best explain the geological observations, using a Markov Chain Monte Carlo (MCMC) inverse method. The outline of this reconstruction process is shown in Fig. 1 for the Ni/Co-Th/Sc ratios, and details of each step of this process are given below. The C++ and Python codes used in this reconstruction are available on the authors' GitHub page (https://github.com/mpptacek/ArchaeanMCMC).

Not all geochemical ratios are suitable for our study. Some ratios do not differentiate between the three endmembers and are thus of no use in a mixing model. Some elements can be mobilized by chemical weathering, affecting the composition of terrigenous sediments. Others can be fractionated in coarse grain sediments that concentrate minerals resistant to weathering and/or that have high density. For these reasons, we use a filtering algorithm to detect sediments that were obviously affected by these processes and remove them from our analysis.

There are two major sources of data for our reconstruction. The first is the igneous rock database from Keller and Schoene (2012) (named 'KS12' hereafter), which was modified by us (named the Origins Lab Igneous Rock Database, or 'OrIgn'; supplementary file mmc6). The second is a terrigenous sediment database compiled from published literature data, containing measurements of shale, loess, and diamictite samples (named the Origins Lab Terrigenous Sediment Database, or 'OrTeS'; supplementary file mmc2).

2.1. Calculating endmember composition

We use the OrIgn database for calculating most endmember compositions. The first step is to extract three subsets from this database: felsic, mafic, and komatiitic rocks. We use the classification scheme of Le Bas and Streckeisen (1991) for this partitioning: rocks with SiO_2 concentrations in the range 63-80 wt.% are classified as felsic, those with <18 wt.% MgO and 45-52 wt.% SiO_2 as mafic, and rocks with >18 wt.% MgO which are also labelled as 'Komatiite' in the database are classified as komatiitic. We remove all records where the major element concentrations sum to less than 98% or more than 102%. For several elements, the reporting of concentrations in the KS12 database used heterogeneous units (ppb, ppm, wt%). These have been corrected in the new database.

The modern mafic endmember requires additional consideration since KS12 contains some mid-ocean ridge basalts (MORBs), whose chemistry differs from basalts found on the continents. The oldest oceanic crust, found in the Mariana trench, is ~170 Myr old; therefore, when calculating the modern mafic endmember, we exclude all rocks younger than 200 Myr from KS12. To compensate for the missing samples, we add data from a separate dataset generated from a query of the PetDB database (http://www.earthchem.org/petdb). This query includes samples from large igneous provinces, volcanic arcs, orogenic belts, volcanic fields, and volcanic provinces, all dated to <200 Myr.

It is well-established that the dominant mafic lithologies on the Earth's continents have changed over time (Keller and Schoene, 2012), mostly due to cooling of the mantle. Rocks from the TTG suite were very common during the Archaean but were replaced by more K-rich granites in the post-Archaean. TTGs are thought to have formed by melting of the oceanic crust in a hot subduction setting possibly similar to the modern setting where the rare adakites are formed (Moyen and Martin, 2012; Deng et al., 2019). To capture the secular evolution in igneous rock compositions through time (see supplementary file mmc3), we use a moving average model with a Gaussian kernel. This allows us to express the concentration of each element in each endmember as a smooth function of time. For every time t, the model computes the concentration of element X as a weighted average of all measurements in the database, $[X]_i$, according to:

$$[X]_t = \frac{1}{\sum_{i=1}^{n} w_i(t)} \sum_{i=1}^{n} w_i(t)\,[X]_i$$

This is done separately for each endmember. The applied weight of sample i, $w_i(t)$, is a Gaussian function of the time difference between the age of the sample (t_i) and the time t:

$$w_i(t) = \frac{1}{\sqrt{2\pi\sigma_B^2}} e^{\frac{-(t_i-t)^2}{2\sigma_B^2}}$$

This function assigns significant weight to samples that are similar in age to t, and a low weight to samples which differ more in age. The parameter σ_B^2 defines the 'bandwidth' of the averaging kernel. We optimize the bandwidth value via a standard k-fold

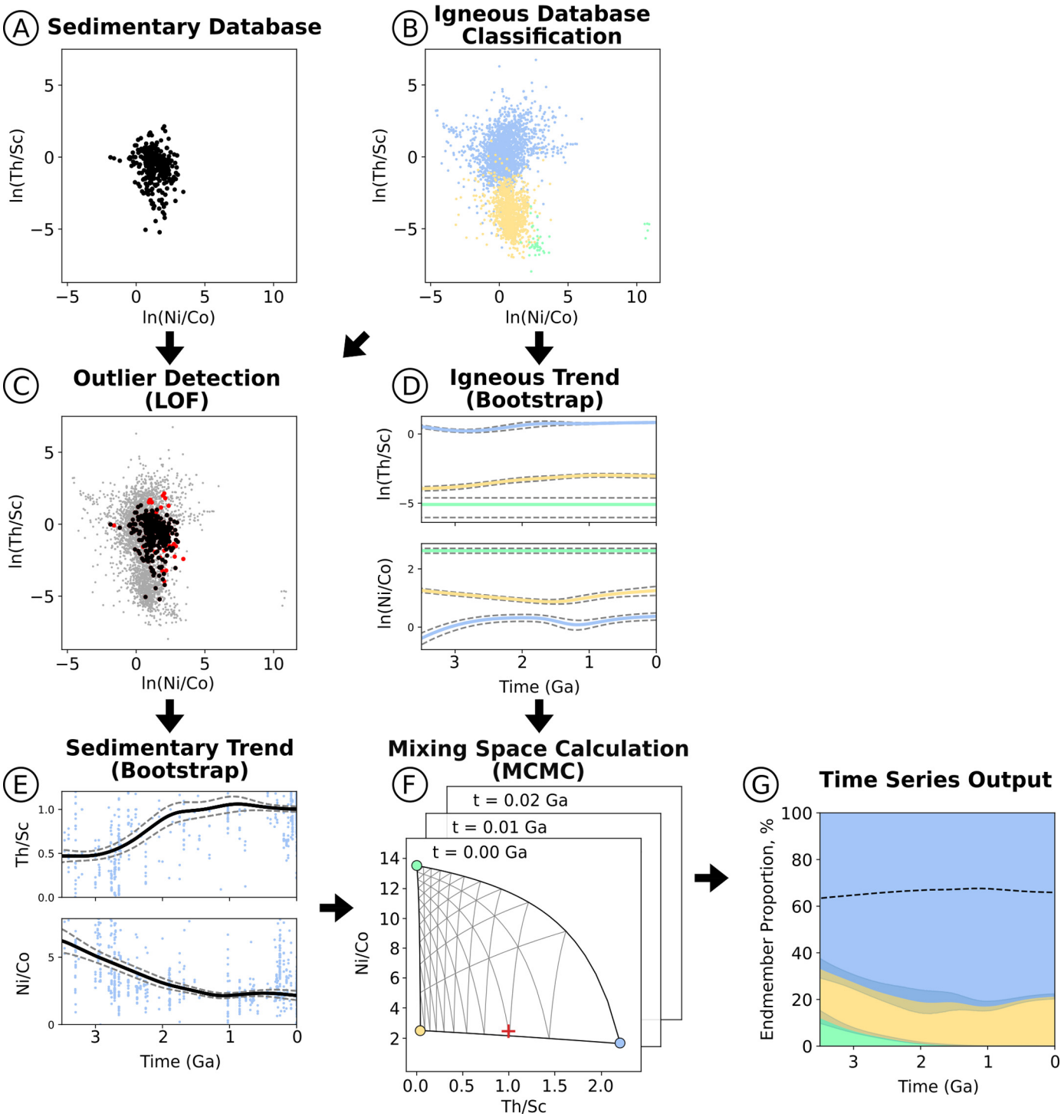

Fig. 1. Graphical overview of the crustal provenance reconstruction process using Ni/Co and Th/Sc ratios as examples. The inputs are two databases: the OrTeS sedimentary database (panel A, supplementary file mmc2) and the OrIgn igneous database (panel B, supplementary file mmc6). The rocks in the igneous database are first sorted into the categories of felsic, mafic, and komatiitic rocks based on their major element chemical compositions (see text and Greber et al., 2017 for details). The average composition of these 'endmembers' through time is computed (D; blue=felsic, yellow=mafic; green=komatiite; Section 2.1; available as supplementary file mmc3). The sedimentary data is filtered for outliers using the local outlier factor (panel C; Section 2.2), then extrapolated to a continuous time series using a bootstrap technique (panel E; Section 2.3). At each time-step, a Markov Chain Monte Carlo (MCMC) technique is used to find what mixture of igneous endmembers (D) best explains the observed sedimentary composition (C) (panel F; Section 2.4). This results in a final time series of best-fitting endmember mixtures through time (G). To find which combinations of geochemical ratios are best suited to reconstructing endmember mixtures, we employed an exhaustive grid search technique (Section 2.5). (For interpretation of the colours in the figure(s), the reader is referred to the web version of this article.)

cross-validation method (see supplementary file mmc1 for details). A value of 1000 Myr is suitable for most elements in our igneous database.

To estimate element ratios and their uncertainties, we use a similar Gaussian moving average model to compute a separate fit for each ratio involved in the reconstruction. For a numerator element A and denominator B, the ratio A/B is computed as:

$$\left(\frac{\mathrm{A}}{\mathrm{B}}\right)_t = \frac{\sum_{i=1}^{n} w_i(t)\,[\mathrm{B_i}]\,(\mathrm{A/B})_i}{\sum_{i=1}^{n} w_i(t)\,[\mathrm{B_i}]}$$

This approach is more robust than computing a moving average of the ratio, since it respects mass-balance.

We then use a bootstrap algorithm (Efron and Tibshirani, 1986) to estimate the confidence interval on the element ratios of the end-members. We generate 10,000 synthetic datasets by drawing with replacement from the original dataset until each synthetic dataset has the same number of samples. We then compute the best fit to each of our synthetic datasets. Finally, for each time t, we compute the standard deviation of all the synthetic best-fit values at that time and use that value as the standard deviation of the endmember ratio at that time. This procedure is performed separately for the felsic and mafic endmembers. Since our databases only contain a limited number of komatiites, we consider the komatiitic endmember composition constant through time (Appendix A; supplementary file mmc6). We do not consider uncertainties in the absolute elemental concentrations.

In Fig. S1 (supplementary file mmc1), we plot the concentrations and selected elemental ratios for Archean igneous rocks aged 3.0-3.8 Ga and compare them with modern igneous rocks from Iceland and the Andes. As illustrated, the majority of Archean rocks follow Andes-like calc-alkaline trends. We make no assumption, however, with regard to the magmatic differentiation series that igneous rocks belong to, as we simply take the average of all felsic rocks in any age interval, regardless of their tholeiitic, calc-alkaline, or alkaline affinities. The only assumption that we make is that the inventory of felsic rocks of any given age available for sampling today is representative of felsic rocks that were exposed to weathering at that time.

2.2. Filtering the sedimentary archive

Terrigenous sediments are the products of chemical and physical weathering of the continents. During soil formation and transport to the oceans, minerals can be altered into new alteration phases, fluid-mobile elements can be leached, and large and/or high-density minerals can be sequestered into coarse grain sediments. After deposition, diagenesis can further modify the concentrations of fluid-mobile elements in the sediments. All these processes can alter elemental ratios such that the final composition of a sediment is no longer representative of its initial source. All studies relying on ancient sedimentary archives are confronted with this complication. To minimize the impact of these effects on our analysis, we filter the sediments in OrTeS to algorithmically identify samples whose compositions have obviously been altered by secondary processes.

In igneous rocks, element ratios are often correlated. Our filtering process was therefore designed to verify that the samples in OrTeS obeyed the same patterns as those found in igneous rocks. We designed a hyperdimensional density-based filter based on the Local Outlier Factor (LOF) algorithm (Breunig et al., 2000) to eliminate samples obviously affected by secondary processes. The first step in this filtering process is to find and rank the chemical ratios that best correlate with the proxy ratios. Algorithmically finding well-correlated ratios is a non-trivial matter, since the correlation metrics most often used in geochemistry are only applicable to monotonic (rank-based Spearman, Kendall) or linear (Pearson) relationships. During magmatic differentiation, however, the compatibility of elements can change depending on the nature of the crystallizing minerals, often creating non-monotonic trends. For this reason, we have chosen to use a popular non-monotonic correlation metric from information theory, the pairwise Mutual Information (MI). MI works by quantifying the difference between the joint distribution of two variables, $f(X,Y)$, and the product of the individual marginal distributions of these variables, $f(X)\cdot f(Y)$. If X and Y are correlated, the joint distribution will be substantially different from the product of the marginal distributions, leading to a high value of MI (and *vice versa*). A graphical example is provided in the supplementary file mmc1 (Fig. S2). MI is unbounded, taking on values between zero (independent variables) and $+\infty$ (strongly dependent variables), which makes its interpretation unintuitive. More conveniently, MI can also be expressed as the MI *generalized correlation coefficient* $r_{MI}(X,Y)$, which takes its values between 0 (independent) and 1 (strongly dependent), and is equal to the Pearson coefficient for a bivariate normal distribution (Lange and Grubmüller, 2006). Hence, MI can be interpreted as a generalization of Pearson's coefficient for non-linear relationships. As an example, the MI algorithm determines that the Th/Sc ratio in igneous rocks is most closely correlated with Nb/TiO_2, Ce/Co, and Hf/Ni ratios.

To apply the LOF algorithm to our data, we first algorithmically select 8 ratios from the pairings of the 16 fluid immobile elements considered in this study (Sc, Cr, Co, Ni, Pb, Zr, Hf, Nb, Ta, Ti, Al, La, Ce, Yb, Y, and Th; see Sect. 2.5 for details on the rationale behind the selection of these elements). This selection always includes the proxy ratios that will later be used in the reconstruction. If less than 8 ratios are used in the reconstruction, we also include additional ratios, chosen by selecting ratios among the remaining elements that best correlate with any of the proxy ratios in the mmc6 igneous rock database. We first create a list of 'candidate' filter ratios containing all possible pairings of the sets of 16 'reliable' elements into 8 ratios. We sort this extensive list of candidates (2,027,025 combinations in total) in order of descending mutual information with the original set of proxy ratios. Since MI is a pairwise metric, we calculate the correlation of each candidate ratio with each proxy ratio separately – our method cannot consider correlations of three or more ratios simultaneously. Then, we repeatedly select the first ratio in this sorted list not containing an element that occurs in one of the previously-selected ratios. For example, if our reconstruction system is Ni/Co+Th/Sc and we want to filter out samples with spurious Th/Sc ratios, we first find the ratio most correlated with Th/Sc that does not include elements Ni/Co, which is Nb/TiO_2 (Fig. S3). The Nb/TiO_2 ratio is added to the filter, and any following ratios are not allowed to contain Th, Sc, Ni, Co, Nb, or Ti. This process is repeated until eight total ratios have been selected, which includes the original proxy ratios. In the context of a Ni/Co+Th/Sc reconstruction, the same approach would be used for detecting spurious Ni/Co ratios.

Once the filtering ratios have been automatically selected, we apply the Local Outlier Filter (LOF) (Breunig et al., 2000; Schubert et al., 2014) to the sedimentary record. The intuition behind the LOF algorithm is straightforward: the average distance of an outlier to its k (we use $k=50$) nearest neighbours should be significantly higher than the average distance between each of those nearest neighbours and their own k nearest neighbours. In other words, the outlier should be in a region in data space that is sparsely populated (low local density) compared to its nearest neighbours. This approach, which relies on a comparison between densities of points and their neighbours, is robust to changes in the average density across different regions. For instance, komatiites are significantly less sampled in geochemical databases compared to basalts, but because their local density is consistent, they will not

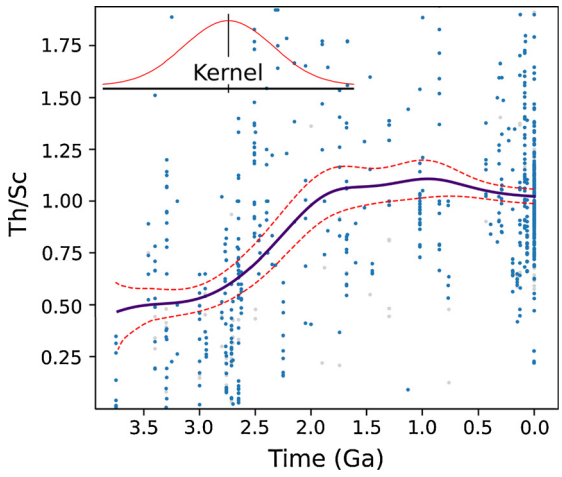

Fig. 2. Example output of the bootstrap algorithm when applied on filtered sedimentary Th/Sc (ppm/ppm) data. Red dotted line represents 95% confidence intervals, thick black line the best fit. The model used was a moving average with a Gaussian kernel of 400 Myr bandwidth (see inset). The blue points are sediment measurements which have been accepted by the LOF filter – grey points have been rejected.

be flagged as outliers (which might happen in a method that only uses global average density). It can also be easily applied to high-dimensional spaces, allowing us to filter using many ratios at once.

Converting a raw LOF score into a binary decision to either eliminate or keep a sample is not straightforward, and several methods exist (Kriegel et al., 2009). For our purposes, we use the OrIgn database as a reference point. To eliminate outliers from the OrTeS database, we first compute the LOF of every point in OrIgn using $k = 50$ nearest neighbours. We use the one-sided 95th percentile of this range as the critical value of our test. For each measurement in OrTeS, we find its k nearest neighbours in OrIgn, compute its LOF, and flag the sample as an outlier if the value is above the critical value. Only samples that are not flagged as outliers are used in the next steps of our calculation.

By construction, applying this filter to igneous rocks would flag 5% of the samples as outliers. Applying this filter to Ni/Co-Th/Sc (and the 6 other ratios automatically selected by our algorithm: Nb/TiO_2, Cr/Ta, Al_2O_3/Pb, Hf/Yb, La/Y, Ce/Zr) in OrTeS flags 9.5% of the samples as outliers, showing that the sedimentary samples show more scatter than igneous rocks, which most likely reflects the imprint of secondary modifications by weathering, transport and diagenesis. As an example, Fig. S3 shows the shale samples detected as outliers for the Th/Sc system.

2.3. Secular evolution in the geochemistry of sediments

The sedimentary rock record is sparsely populated and contains significant gaps in time. Moreover, individual sediment compositions can be influenced by local drainage basins rather than large swaths of emerged continents, meaning they might not necessarily resemble the global average. To resolve these problems, we estimate the global average composition for each ratio with as much data as possible. To this end, we use a Gaussian moving weighted average model similar to that used for endmember compositions (see Sect. 2.1 for details). This allows us to compute a smooth, continuous best-fit to the sparse sedimentary data. In this case, we use a kernel bandwidth of 400 Myr. Applying the same bootstrapping procedure to the sediments as we did to the endmember concentrations, we compute both the best-fit and 95% confidence intervals for the proxy ratio as smooth functions of time. An example output of this procedure is shown in Fig. 2.

2.4. Markov chain Monte Carlo inversion

Using the quantities estimated above, we calculate, at each age, what mixture of the felsic, mafic, and komatiitic endmembers best reproduces the sediment proxy ratio data. This is achieved by minimizing the misfit between the calculated and observed sedimentary compositions. The misfit is quantified using the χ^2 error function:

$$\chi^2 = \sum_{j=1}^{m} \frac{\left(R_j^o - R_j^*\right)^2}{\sigma_j^2}$$

where R_j^o is the value of the j^{th} observed geochemical ratio in sediments, R_j^* is the prediction of our mixture model, and σ_j^2 the effective variance of that ratio (described below).

Defining p_F, p_M, and p_K as the fractions of the felsic, mafic, and komatiitic endmembers in the upper continental crust at a given time, we can write the model predicted value of the j^{th} ratio as,

$$R_j^* = \frac{1}{\sum v}\left\{ v_K \left(\frac{A}{B}\right)_{Kj} + v_M \left(\frac{A}{B}\right)_{Mj} + v_F \left(\frac{A}{B}\right)_{Fj} \right\},$$

with the coefficients,

$$v_K = p_K[B_{Kj}];\ v_M = p_M[B_{Mj}];\ v_F = p_F[B_{Fj}].$$

An additional constraint arises from the fact that the contributions of the three endmembers must sum to 100% ($p_F + p_M + p_K = 1$). To solve this system of equations for three endmembers, at least two proxy ratios are required. The values p_K, p_M, and p_F are the model parameters, and the proxy ratios (R_j^o) are the observed values that the model is trying to reproduce. In a simple regression, we would only have uncertainty in the observations. However, here we also have uncertainties in the model, since we do not have exact knowledge of the endmember compositions (estimated in Sect. 2.1). One way to calculate the uncertainty in this context is the effective variance method, which considers variance in both the model parameters and the observations. The effective variance of the j^{th} ratio is:

$$\sigma_j^2 = \sigma_{sj}^2 + \left(\frac{v_K}{\sum v}\right)^2 \sigma_{Kj}^2 + \left(\frac{v_M}{\sum v}\right)^2 \sigma_{Mj}^2 + \left(\frac{v_F}{\sum v}\right)^2 \sigma_{Fj}^2$$

where σ_{sj} represents the uncertainty in the sedimentary signal, and σ_{Kj}, σ_{Mj}, σ_{Fj} are the uncertainties in the komatiitic, mafic, and felsic endmembers, respectively. These uncertainties are estimated by the bootstrap algorithm and change as a function of time. We did not propagate uncertainties in the absolute concentrations, only in the ratios. To minimize the χ^2 misfit and calculate the confidence intervals of the fit parameters (p_K, p_M, and p_F), we use the Metropolis-Hastings algorithm (Metropolis et al., 1953), which belongs to the class of Markov Chain Monte Carlo (MCMC) computational methods.

For each geological time, 1.5 million iterations of the Metropolis-Hastings algorithm are executed. We record the Markov Chain state at every iteration and keep track of the state with the lowest χ^2 (the best fit). The first fifth of the Markov Chain states (300,000 iterations) is discarded (to allow for burn-in), and the rest are used to calculate the confidence interval of the endmember. We have verified that the Markov Chain converges to its equilibrium distribution within two hundred iterations, ensuring our confidence interval estimates are accurate (Fig. S4). We run this procedure with a 10 Myr timestep starting from the earliest time when sedimentary data is available (usually around 3.5 Ga, though this depends on the ratios used).

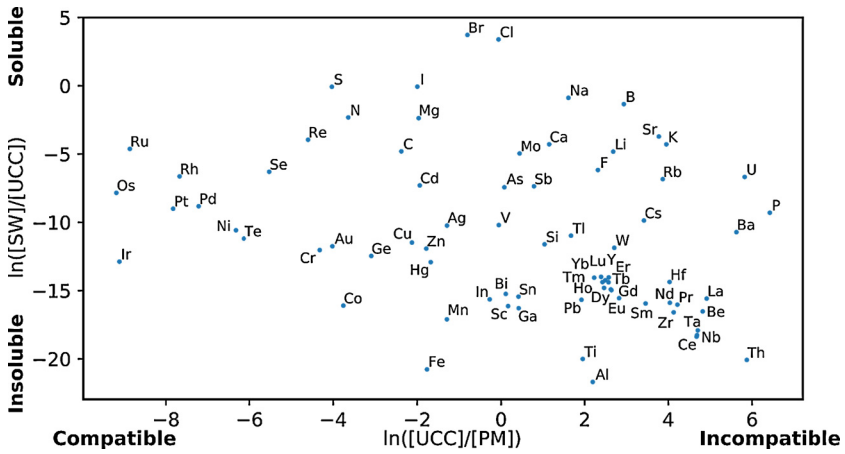

Fig. 3. Metrics of solubility in aqueous medium against igneous compatibility for most naturally-occurring elements. Solubility is roughly quantified as the natural logarithm of the ratio of the elemental concentration in seawater (SW) to that in the upper continental crust (UCC). Igneous compatibility is quantified as the logarithmic ratio of UCC to primitive mantle (PM) concentrations. The ideal combination of proxies for reconstructing the continental crust will contain elements that are insoluble and span a wide range of igneous compatibility. Such a combination will make it easy to distinguish between komatiite, mafic, and felsic rocks. See text for a more in-depth discussion of element suitability. Primitive mantle concentration data from McDonough and Sun (1995); upper continental crust data from Wedepohl (1995); average seawater concentrations from Bekov et al. (1984), Nozaki (1997), and Sohrin et al. (1998).

2.5. Proxy ratio search

As previously discussed, not all ratios are well suited for our reconstruction. The suitable elements should (*i*) have low aqueous solubility so that they are minimally affected by weathering, (*ii*) not be concentrated in especially resistant or dense minerals so that they are not fractionated during transport, and (*iii*) span a wide range of concentrations in the igneous endmembers considered. Figure 3 shows a plot of aqueous solubility (roughly quantified using the ratio of the concentration in the oceans to the continental crust) against igneous compatibility (quantified using the ratio of the concentration in the continental crust to the primitive mantle). No element completely fulfils all our criteria; hence, some compromise must be sought.

On the modern Earth, the elements that have low apparent solubility (from low to high) are Fe^{3+}, Th, Al, Sc, REEs, Co, $Mn^{3+,4+}$, Pb, Be, Sn, Zr, Nb, Y, Ti, Ga, Hf, In, Ta, Zn, Cu, Cr^{3+}, and Ge. In the Archaean ocean, Fe and Mn existed mostly in the soluble Fe^{2+} and Mn^{2+} oxidation states, and are therefore unreliable proxies.

The elements that are the most compatible in olivine, namely Sc, Cr, Co, Ni, and the Platinum Group Elements (Ru, Rh, Pd, Os, Ir, Pt – 'PGEs') will be most diagnostic of the contribution of komatiitic and mafic rocks. The PGEs are concentrated in trace minerals and can be segregated into heavy minerals. Furthermore, a significant proportion of the PGEs is delivered to sediments by extra-terrestrial sources, also rendering them unsuitable for our purposes. The elements that are the most incompatible will be most diagnostic of felsic input. Large ion lithophile elements (K, Rb, Cs, Sr, Ba, Pb, and Eu^{2+}) are highly incompatible, but usually also rather soluble – hence, they are unsuitable for our purposes. Pb is very particle reactive and has a low residence time in the oceans. Other elements that are incompatible and have low solubility in seawater are the High Field Strength Elements (Zr, Hf, Nb, Ta, Ti), the Rare Earth Elements, Y, and Th. Among the REEs, we use the insoluble light REEs La and Ce. In the Archean, Ce existed as Ce^{3+} whose solubility was presumably similar to insoluble La^{3+}. Under modern oxic conditions, Ce can be oxidized to 4+, which is even less soluble.

Considering all the criteria, the insoluble elements that should be the most reliable and discriminating are Sc, Cr, Co, Ni (compatible), Pb, Zr, Hf, Nb, Ta, Ti, Al, La, Ce, Yb, Y, and Th (incompatible). One aspect not addressed in this selection is the issue of mineral fractionation during transport. Indeed, some of the elements identified above are concentrated in very fine alteration minerals (*e.g.*, Al in clays), while others are concentrated in large detrital minerals (*e.g.*, Zr and Hf in zircons). Greber and Dauphas (2019) examined this question by tracking the evolution of the Zr/Al ratio in terrigenous sediments through time. They found that the effect of mineral fractionation was relatively minor, and reconstructions involving ratios potentially fractionated by mineral sorting (Al_2O_3/TiO_2 or Zr/TiO_2) yielded results similar to other ratios. Our analysis also shows that the reconstruction of the continental crust composition does not depend much on the choice of the proxy ratio. As discussed in Sect. 3, application of the inversion algorithm to recent sediments yields a model continental crust composition that agrees with independent estimates. Its application to diamictites also yields results that are consistent with those inferred from shales of the same age. We have also performed an inversion excluding 4 elements that could be prone to mineral sorting (Zr, Hf, Ce, and Yb) and find that the reconstructed composition of the upper continental crust is little changed compared to that inferred when those elements are included (Fig. S5). We therefore conclude that while mineral sorting during transport is expressed in shales, its effect on the inversion is small and does not affect our conclusions. Furthermore, the chemical compositions of sediment samples strongly affected by mineral sorting would move away from the trend defined by igneous rocks and the samples most affected would be detected as outliers by the LOF algorithm (Sect. 2.2).

There are many possible ways to combine the 16 elements selected into a set of ratios (see Appendix B for a derivation of the underlying combinatorics). Using two ratios in the reconstruction, the number of potential combinations is 5,460. Using six ratios, there are 18,918,900 possible choices, and for eight ratios (*i.e.*, including all suitable elements) there are 2,027,025 choices. Geochemical intuition and previous work tell us that some combinations of ratios are better suited than others to reconstruct the composition of Earth's crust. An example comparison is shown in Fig. 4: the Ni/Co+Th/Sc mixing system is well-formed and can clearly differentiate between the three endmembers, while the Cr/V + Ni/Co system is degenerate and small uncertainties in the shale/diamictite composition will result in large uncertainties in the calculated endmember proportions.

To objectively rank which combinations of elemental ratios are most useful, we applied our inversion algorithm to three synthetic sedimentary compositions (*e.g.*, Fig. 4). Two of these compositions

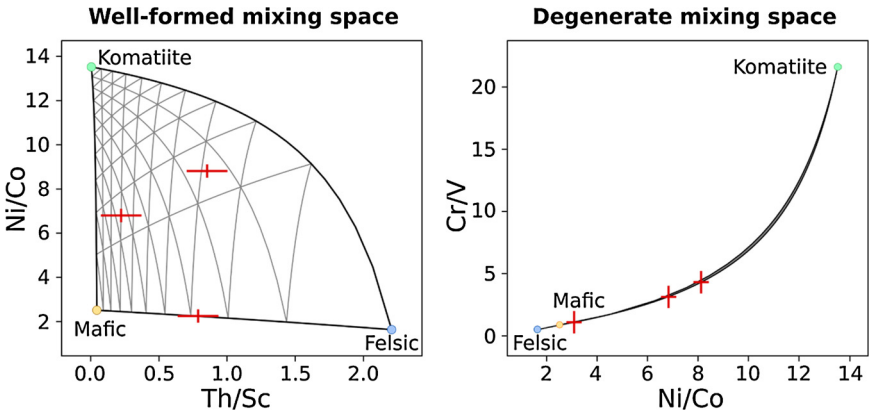

Fig. 4. Illustration of our approach to find the best-formed mixing space (Sect. 2.5; Table 1). We performed an exhaustive search of all possible combinations of selecting n ratios from a set of 16 elements (Sc, Cr, Co, Ni, Pb, Zr, Hf, Nb, Ta, Ti, Al, La, Ce, Yb, Y, and Th) for values of n between 2 and 8. For each mixing space, we input three synthetic test points, with variances (shown as red crosses) corresponding to the real-world variances of those ratios in our sedimentary database. We then run our reconstruction algorithm on these synthetic test points, using real endmember compositions, and calculate how accurately the rock proportions are recovered by the inversion. In the degenerate example (right), even small uncertainties in the synthetic test points lead to a large deviation in the predicted endmember contributions. The well-formed system (left) is ranked 21/5460 by the algorithm.

Table 1
Combinations of proxy ratios that best recover their synthetic input, sorted by the number of ratios. Our proxy rating metric is based on supplying our reconstruction algorithm with a set of three synthetic inputs (Fig. 4) and determining how accurately and precisely the procedure recovers them. See Section 2.5 for a detailed explanation.

Number of ratios	Possible combinations	Best system
2	5,460	Ni/TiO_2, Sc/Zr
3	120,120	Al_2O_3/TiO_2, Ni/Y, Sc/Zr
4	1,351,350	Al_2O_3/TiO_2, Ni/Yb, Sc/Zr, Ta/Th
5	7,567,560	Al_2O_3/TiO_2, La/Yb, Ni/Y, Sc/Zr, Ta/Th
6	18,918,900	Al_2O_3/TiO_2, Co/Ni, Cr/Yb, La/Y, Sc/Zr, Ta/Th
7	16,216,200	Al_2O_3/La, Ce/Y, Co/Ni, Cr/Yb, Hf/TiO_2, Sc/Zr, Ta/Th
8	2,027,025	Al_2O_3/La, Ce/Y, Co/Ni, Cr/Yb, Hf/TiO_2, Nb/Pb, Sc/Zr, Ta/Th

were generated using Archaean-age endmembers in proportions suggested by Greber et al. (2017) and Tang et al. (2016), respectively representing a mostly-felsic and a mostly-mafic emerged crust (with proportions of 15/27/58% and 15/70/15% komatiite/mafic/felsic). The third synthetic sedimentary composition is similar to the present-day composition of the continental crust (28% mafic and 72% felsic mixture of modern endmembers). We artificially added noise to these synthetic compositions so that the variance in the synthetic input matched the real-world variance seen in OrTeS. We then ran the MCMC inversion on the synthetic data, and rejected those combinations of ratios that did not recover the original inputs. Next, we took the maximum predicted uncertainty from these three cases and used it to rank the combinations of ratios, ranking combinations with the lowest uncertainty as the best. After exhaustively applying this test to all 46.2 million possibilities, we found the best combinations of ratios for every number of ratios from two to eight (listed in Table 1; see supplementary file mmc4 for an extensive list of all the rankings). The best set of 2 ratio proxies is Ni/TiO_2 and Sc/Zr. To our knowledge, these two ratios have not been used previously in provenance studies, illustrating the virtue of algorithmically searching for the element ratios that are best suited to do the inversion. This algorithmic selection, however, does not run against geochemical intuition. Indeed, Ni is highly compatible and is concentrated in komatiites relative to mafic and felsic rocks while Ti is incompatible during mantle melting and thus enriched in mafic rocks relative to komatiites (Fig. 3). The Ni/TiO_2 ratio is thus a good discriminator of the contribution of komatiites. Zirconium is highly incompatible relative to Sc (Fig. 3) and the Sc/Zr ratio thus distinguishes between felsic and mafic rocks. The element ratios that have been traditionally used to infer the nature of the provenance of terrigenous sediments are ranked high by our algorithm. For example, the Ni/Co ratio used by Tang et al. (2016), Greber et al. (2017) and Greber and Dauphas (2019) first appears in the 2-ratio ranking paired with the Sc/Zr ratio at rank 11/5460. The Th/Sc ratio used by Taylor and McLennan (1985) and Greber and Dauphas (2019) first appears paired with the Cr/TiO_2 ratio at rank 7/5460 (Th/Sc+Ni/Co is ranked 21/5460). The Al_2O_3/TiO_2, Zr/TiO_2, and La/Sc used by Greber and Dauphas (2019) are paired in our highest ranking with Ni/Co (ranked 232/5460), Ni/Yb (9/5460), and Ni/Co (670/5460), respectively. Note that the selection of the ratio by the algorithm does not depend solely on whether the topology of the mixing curves is the most discriminant (Figs. 1, 4), which can be tackled in part by geochemical intuition, but also on whether the ratios are well determined and have little analytical or geologic scatter, which is more difficult to assess other than algorithmically. The best set of 8 ratio proxies (Al_2O_3/La, Ce/Y, Co/Ni, Cr/Yb, Hf/TiO_2, Nb/Pb, Sc/Zr, and Ta/Th) should provide the least biased estimate of the nature of the provenance as the different ratios are potentially sensitive to different biases.

3. Results

We used our novel reconstruction pipeline to re-process sediment geochemistry data which had previously been used to argue for a mafic Archaean emerged crust. Our reconstruction indicates that sedimentary data are consistent with an upper continental crust containing >50% felsic material at 3.5 Ga.

We also used combinations of geochemical ratios found to be the most diagnostic based on our algorithmic approach. In all cases, these 'best' systems point to a predominantly felsic Archaean (Fig. 5). The reconstructed composition of the Earth's emerged

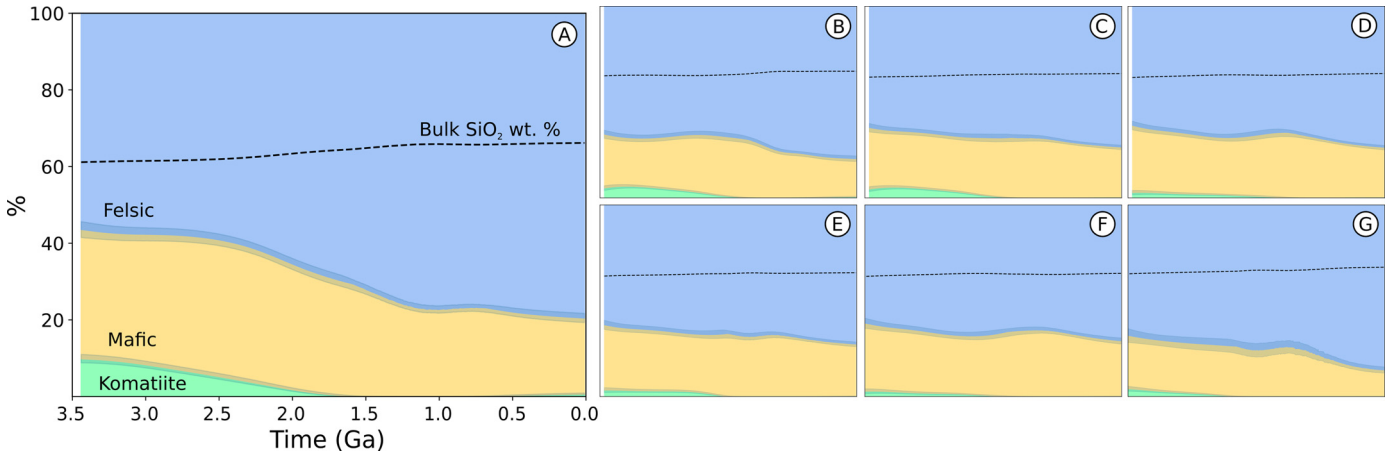

Fig. 5. Reconstructed contribution of felsic, mafic, and komatiitic material to the upper continental crust as a function of time, according to several different systems of proxy ratios. (*A*) The best eight-ratio system Al_2O_3/La, Ce/Y, Co/Ni, Cr/Yb, Hf/TiO_2, Nb/Pb, Sc/Zr, Ta/Th. (*B*) The best seven-ratio system Al_2O_3/La, Ce/Y, Co/Ni, Cr/Yb, Hf/TiO_2, Sc/Zr, Ta/Th. (*C*) The best six-ratio system Al_2O_3/TiO_2, Co/Ni, Cr/Yb, La/Y, Sc/Zr, Ta/Th. (*D*) The best five-ratio system Al_2O_3/TiO_2, La/Yb, Ni/Y, Sc/Zr, Ta/Th. (*E*) The best four-ratio system Al_2O_3/TiO_2, Ni/Yb, Sc/Zr, Ta/Th. (*F*) The best three-ratio system Al_2O_3/TiO_2, Ni/Y, Sc/Zr. (*G*) The best two-ratio system Ni/TiO_2, Sc/Zr.

crust is consistent with the conclusions drawn from Ti isotope systematics (Greber et al., 2017) and element ratios Al/Ti, Zr/Ti, La/Sc, Th/Sc, Cr/Sc, and Ni/Co (Greber and Dauphas, 2019). The early Archaean continental crust was 56 ± 2% felsic, 34 ± 2% mafic, and 10 ± 1% komatiite, resulting in a global SiO_2 concentration of 61 wt.%. This result does not depend on the choice of proxies used in the reconstruction (including those previously used to argue for an early mafic crust). We validated our results by verifying that for the modern, our algorithm yields an emerged crust composition corresponding to the modern emerged crust. We calculate that in the modern, the emerged crust should be 80 ± 2% felsic and 20 ± 2% mafic with a global SiO_2 concentration of 66 wt.%, in agreement with independent estimates (Condie, 1993; Rudnick and Gao, 2003). The predicted negligible contribution of komatiite to the modern continents is a natural conclusion of our data; we do not artificially force our calculation to reduce komatiite as a function of time. Our reconstructed composition for the Archaean is in good agreement with a study that inventoried rocks of Archaean age and concluded that they comprise 75% felsic, 18% mafic, and 7% komatiite rocks (Condie, 1993). This suggests that there is no strong preservation bias for or against felsic rocks.

Gaschnig et al. (2016) argue that diamictites may be more reliable proxies of crustal composition, since (*i*) they are less affected by mineral sorting, and (*ii*) low-temperature glacier alteration is less likely to mobilize fluid-mobile elements. In theory, our LOF filter should remove shale compositions most modified by secondary processes, and thus our results should not be too affected by mineral sorting or chemical alteration. We investigated the suitability of diamictites as proxies for the emerged crust by separating the shale and diamictite samples in the OrTeS database into two separate subsets and running a reconstruction using only the diamictite samples. We found no statistically significant difference from the reconstructions based only on shales. Diamictites may offer a less altered view of the crust composition than shales but since the results of our algorithm are the same with diamictites as with shales, we posit that using both simultaneously is the preferred approach, especially since shales are much more abundant in the geological record.

4. Discussion

Our reconstruction predicts that the ratio of mafic to felsic rocks in the crust has remained mostly steady through time. Though komatiites have disappeared gradually through time, they have mostly been substituted by mafic rocks. As discussed by Greber et al. (2017), this finding is consistent with the operation of subduction and possibly plate tectonics before 3.5 Ga.

Because the average compositions of the endmembers themselves have changed through time, we predict that the average concentrations of some elements in the continents (for example P, K, Mg, U, Th, Ni, Cr, and Co) have undergone significant changes (Fig. 6; Fig. S6; supplementary file mmc5). These changes could have had significant impact on the surface environment. For instance, high concentrations of Mg in the Archaean (2.6 times the modern value) might have caused much more extensive dolomitization, as it would have increased Mg concentrations in seawater. The changing concentrations of species important for radioactive dating, such as ^{176}Lu -^{176}Hf, ^{147}Sm -^{143}Nd, and ^{87}Rb -^{87}Sr (Figure S7), could also influence calculations of model ages of mantle extraction. Other implications of how a changing chemistry of the continents might have affected surface conditions and life are discussed in Greber et al. (2017). Below, we focus on determining why our results differ from some earlier studies, despite using the same observations, and the possible implications of our results on the thermal structure of the Archaean continental crust.

4.1. Comparison with earlier studies

Several previous studies have used elemental ratios to infer the nature of the Earth's emerged crust in the Archaean. Most of these studies remained qualitative, merely pointing out that some ratios were closer to the mafic endmember and therefore that the Earth's emerged crust must have been more mafic. The ratios discussed in that context were La/Sc, Th/Sc, ΣLREE/ΣHREE (Taylor and McLennan, 1985); Cr/U (Smit and Mezger, 2017); Th/Cr, La/Cr, ΣLREE/ΣHREE (Large et al., 2018); and Ni/Lu, Th/Sc, Eu/Eu* (Gaschnig et al., 2016). Tang et al. (2016) and Chen et al. (2019) applied a more quantitative approach to this problem by using the Ni/Co, Cr/Zn, and Cu/Al_2O_3 ratios with the aim of reconstructing the composition of the Earth's crust.

In many of these studies, the continental crust is thought of as being composed of mafic and felsic lithologies (Large et al., 2018; Smit and Mezger, 2017). The problem with this approach is that the Archaean crust comprised significant amounts of komatiite, which are very enriched in elements that are compatible in olivine (notably Cr, Ni and Co). Hence, certain secular trends that were previously interpreted to reflect a greater proportion of mafic lithologies instead reflect the greater contribution of komatiites. Another potential pitfall is that some of the elements used are either very soluble (U) or mildly insoluble (Zn), and the sol-

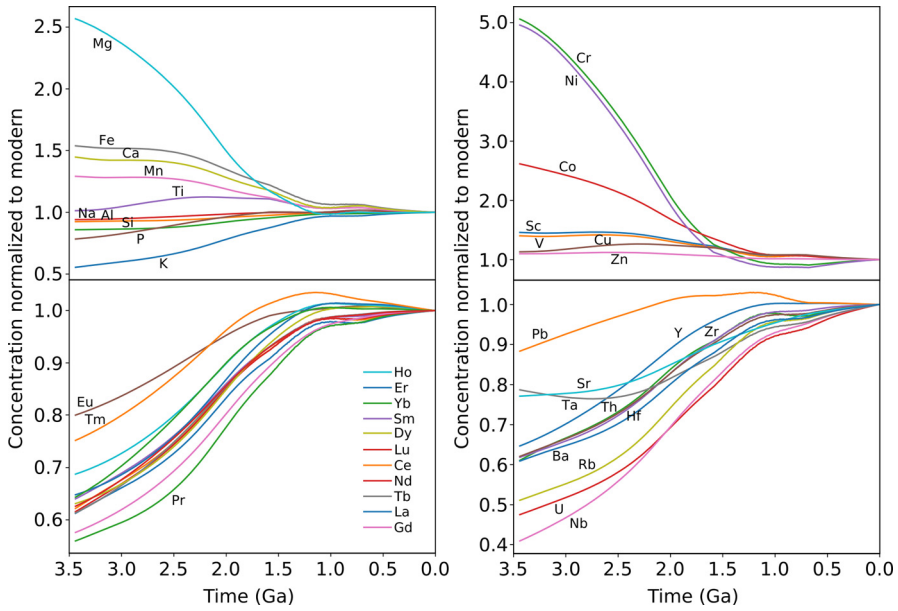

Fig. 6. Reconstructed concentrations of selected elements through time in the Earth's upper continental crust normalized to calculated modern-day values (supplementary file mmc5). This reconstruction used the best eight-ratio combination, thereby using as much information as possible to obtain the most robust result. The concentration of Si in the upper crust increased from 61% to 66% since 3.5 Ga, indicating that despite the observed changes in the concentrations of many major, trace, and rare earth elements, the crust has remained predominantly andesitic over the last 3.5 billion years. The main driver of change in elemental concentrations is the changing composition of both mafic and felsic rocks through time (due to the secular cooling of the Earth) and the greater proportion of komatiites in the Archaean, rather than a change in the relative proportions of felsic and mafic material.

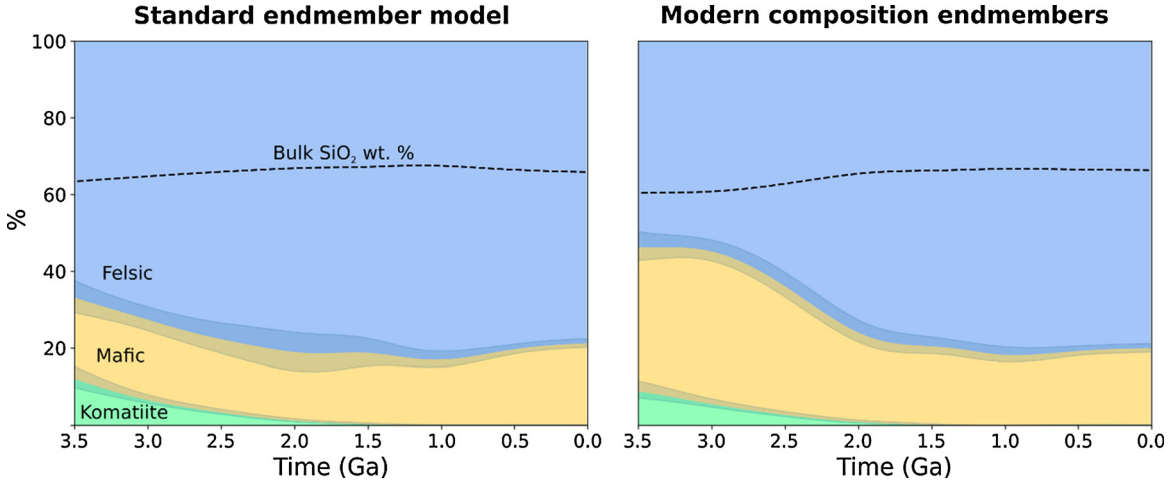

Fig. 7. The results of running a Th/Sc + Ni/Co reconstruction with our time-variant endmember model (left), and with a time-invariant endmember model based only on modern rocks, effectively ignoring the changes in the composition of igneous rocks over the last several billion years (right). Ignoring this change in the composition of igneous rocks introduces a strong bias towards mafic in the Archaean.

ubilities of some of these elements are highly sensitive to the redox state of the oceans and changed at the GOE and the Neoproterozoic oxidation event (*e.g.*, U and Cr). Using soluble elements increases the probability that the sedimentary data may have been affected by chemical weathering. Furthermore, several of these studies did not take into account the fact that the compositions of igneous endmembers changed with time. Archaean mafic rocks were produced by higher degrees of partial melting and were less enriched in incompatible elements than their modern equivalents (Keller and Schoene, 2018). Felsic rocks were dominated by TTGs and are now dominated by granites (Condie, 1993 and references therein). Ignoring the changes in endmember composition introduces a strong bias towards mafic in our reconstruction (Fig. 7) and explains why some previous studies obtained a more mafic Archaean emerged crust.

The study of Tang et al. (2016) most resembles ours in its approach, as it considers changes in the composition of the endmembers through time and the presence of komatiites in the Archaean rock record. Though the authors concluded that rocks exposed to weathering were predominantly mafic, they also ascribed very large uncertainties to their reconstruction. Furthermore, their predicted crustal MgO concentrations generally agree with ours for the entirety of the Archaean.

Chen et al. (2019) used the Cu/Al_2O_3 ratio of diamictites to argue for a predominantly mafic crust at 2.9 Ga. They find an average Cu/Al_2O_3 (ppm/wt%) ratio of ~4.4 in ~2.98 Ga diamictites from the Kaapvaal craton while diamictites ~2.4 Ga or younger have lower values of ~2.1 to 1.0. As shown in Figure S8, our compilation of shale and diamictite compositions does not show such a decrease. Furthermore, the shale+diamictite record of Cu/Al_2O_3 ratios is well reproduced by our 3 component mixing model in-

volving a predominantly felsic crust. The discrepancy with Chen et al. (2019) could be due to the fact that the ~2.98 Ga diamictites with an elevated Cu/Al_2O_3 ratio are all from the Kaapvaal craton and may provide an unrepresentative view of the Archean crust, while shales provide a temporally and geographically more diverse record of the emerged crust.

4.2. Implications for the thermal structure of Archaean continental crust

Heat-producing elements K, U, and Th are highly incompatible, and thus enriched in felsic rocks. As a result, about half of the surface heat flux at the surface of the modern continental crust is attributable to the decay of radioactive elements K, U, and Th within the crust while the other half comes from the mantle (Jaupart et al., 2015). Heat production in the continental crust would have been very different if it was predominantly mafic (Large et al., 2018; Smit and Mezger, 2017; Sun, 2018; Tang et al., 2016; Chen et al., 2019) or felsic (this study; Greber et al., 2017; Greber and Dauphas, 2019). Below, we use our reconstruction of the secular evolution of the concentration of K, U, and Th to calculate the continental geotherm between 3.5 Ga and present, following the methods and assumption of Rudnick et al. (1998). Note that this approach is uncertain as the results depend on the thickness of the Archaean crust and lithospheric mantle, as well as the composition of the crust at depth, which are all very poorly constrained.

If the concentrations of K, U, and Th in the crust were only affected by radioactive decay, calculated backwards from their present-day values, the rate of heat production from radioactive decay would have been 2.75 times today's levels at 3.5 Ga (Fig. 8a). However, our reconstruction shows that the crustal concentrations of K, U, and Th were substantially lower in the past compared to the present (Fig. 8b). Accordingly, our prediction is that in the Archaean crust, the rate of heat production from radioactive decay was only 1.5 times today's level (Fig. 8c).

Due to the secular cooling of the Earth, mantle temperatures were higher than present during the Archaean. To quantify the relative contribution of these two effects (higher radioactive heat production and higher mantle potential temperature), and thereby produce an estimate of the geotherm for the Archaean continents, we constructed a numerical model of heat transfer in the lithosphere. In modern continents, the thermal structure shows great variability (Chapman, 1986). With this caveat in mind, we model only a single representative column of crust using the steady-state heat transport equation:

$$K\frac{d^2T(z)}{dz^2} = -\frac{Q(z)}{\rho}$$

where z is the depth below the surface (in m), T the temperature (in K), Q the amount of heat production (in W/kg), ρ the material density (in mg/m^3), and K the thermal conductivity (W.K^{-1}.m^{-1}). The boundary conditions for this equation are typically specified in terms of heat flux at the surface and at the base of the lithosphere (Rudnick et al., 1998). However, while there are estimates of modern and Archaean mantle temperatures inferred directly from the chemistry of erupted lavas, the heat flux at the base of the lithosphere is more difficult to constrain. Hence, we defined our boundary conditions using absolute temperature instead of heat flux. We fixed the surface temperature at 288 K, and the lithospheric temperature at 1539 and 1739 K for the present day and early Archaean respectively, reflecting the fact that the mantle potential temperature could have been 200-300 K higher in the Archaean than present (Herzberg et al., 2010). We set the crustal thickness as 41 km, and the lithospheric thickness as 125 km.

We use the parameters from Rudnick et al. (1998) for thermal conductivity, density, and relative variation in radioactive element

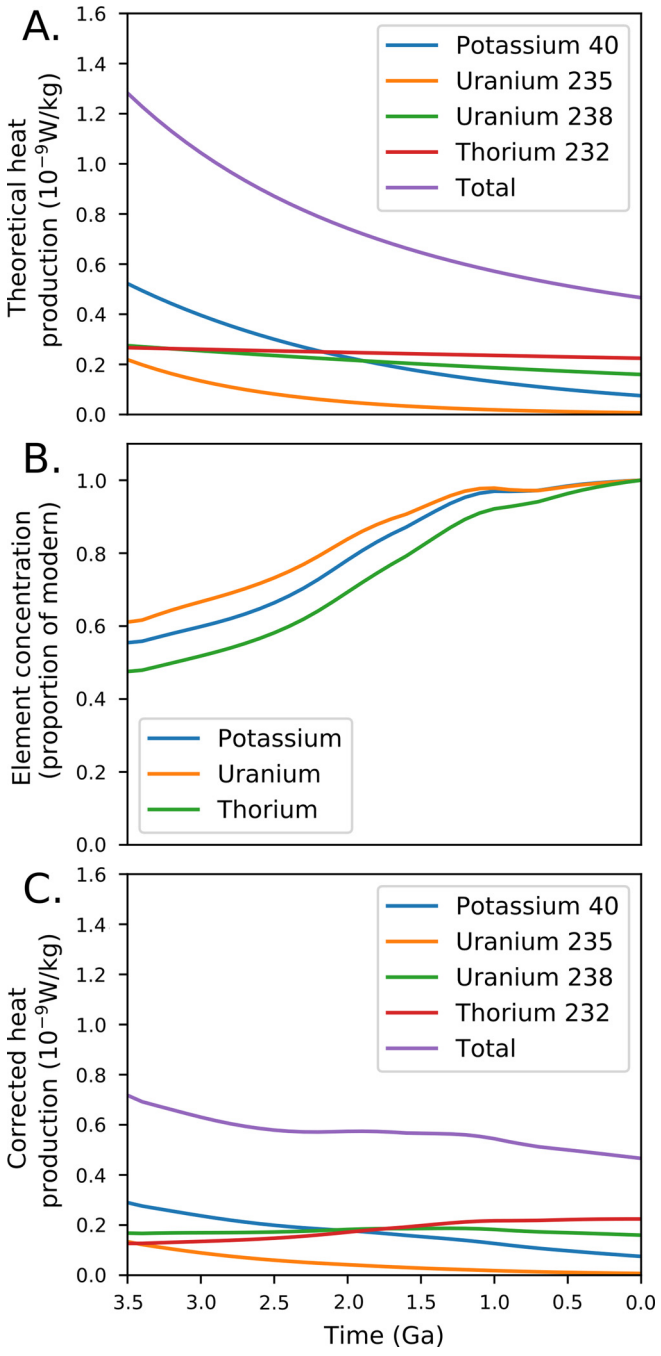

Fig. 8. Changes in crustal radiogenic heat production through time. (a) Predicted contributions of K, Th, and U to crustal heat production, in a hypothetical scenario where their crustal concentrations remained constant through time. (b) Relative changes in the concentrations of these elements through time normalized to the present-day values, as predicted by our reconstruction. (c) Our estimate of actual crustal radiogenic heat generation based on the changes in concentration given by our reconstruction, constructed by multiplying (a) with (b). Note that the amount of heat produced by radioactive elements in the continental crust is predicted to have decreased by around 50% over the last 3.5 Ga.

concentration with depth. Their model supposes that 44% of the total radiogenic heat production occurs in the upper third of the crust, 46% in the middle, and 10% in the lower third. We also used their value of radiogenic heat production in the lithospheric mantle. We then substituted the estimates of total crustal heat production derived from our MCMC reconstruction: 4.66×10^{-10} W.kg^{-1} for the modern, and 7.17×10^{-10} W.kg^{-1} for the early Archaean. Since our reconstruction can only estimate the composi-

tion of the upper crust, we assume that changes in concentrations of elements in the lower crust scale proportionally with those in the upper crust.

For the modern day, our model reproduces contemporary measurements of continental heat flux, yielding a value of 60 mW.m^{-2} as compared to global average of ~65 mW.m^{-2} (Jaupart et al., 2015 and references therein). The calculated near-surface thermal gradient is 20°C.km^{-1}. When brought into the Archaean, our calculation predicts a surface heat flux of 84 mW.m^{-2}, and a near-surface gradient of 28°C.km^{-1}, consistent with the earlier estimates of Rudnick et al. (1998). The model also predicts a Moho temperature of 963 K in the Archaean, compared to 835 K in the modern. Of this 130 K difference in temperature, our model indicates that 40% is attributable to increased mantle temperatures, and 60% to the increased crustal radiogenic contribution.

The thermal gradient ($\Delta T/\Delta P$) recorded by metamorphic rocks of various ages spanning ~3 Gyr of Earth's history has been used to argue for a relatively late and progressive onset of modern-style plate tectonics (Brown and Johnson, 2018; Holder et al., 2019). It relies on the finding that the modern-day bimodal distribution between (1) cold subduction-related thermal gradients and (2) hot thermal gradients away from subduction zones was only progressively established over a time span of 2.6 Gyr. Our geotherm calculation shows that little change is expected in the thermal gradient away from subduction zones, consistent with the finding by Brown and Johnson (2018) and Holder et al. (2019) that the mode in the distribution of $\Delta T/\Delta P$ values of metamorphic rocks corresponding to hot geotherms did not change with time. Their results, however, are also consistent with shallower, hotter subduction in the Archaean, which we argue may be called for by the dominance of felsic rocks at the surface of continents (this study; Greber et al., 2017; Greber and Dauphas, 2019).

5. Conclusions

Ratios of selected elements have previously been used to argue for a predominantly mafic crust in the Archaean. After a re-analysis of published literature data, we demonstrate that measurements once taken as evidence for a mostly mafic crust are instead consistent with a felsic upper continental crust during the Archaean. Such a large felsic contribution to the upper crust is best explained if subduction and possibly plate tectonics were already well-established on the Earth during the early Archaean. Finally, we present a model for the thermal structure of Archaean continental crust based on our geochemical findings.

The conclusions reached in this study rely on the use of several statistical tools that (1) detect sedimentary samples that have been severely compromised by chemical and physical weathering processes, applying a nearest neighbour filtering algorithm, (2) delineate the evolution of proxy ratios in sediments through time by using a non-parametric moving average model and assessing the uncertainty using a bootstrap method, (3) assess the contributions of the three endmember rock types (mafic, felsic and ultramafic) using a MCMC approach to quantify the uncertainties of the best fit parameters, and (4) objectively identify which elemental ratios are best suited for reconstructing the proportions of the three endmembers in the continents through time. This work therefore underlines the value of data-driven advanced quantitative and statistical methods within the field of elemental geochemistry.

Credit author statement

Ptáček and Dauphas conceived the study; Ptáček carried out the analysis and geotherm calculation with guidance from Dauphas; Ptáček, Greber, and Dauphas compiled the databases with the assistance of Hannah Hilbert-Wolf; Ptáček and Dauphas wrote the first draft of the manuscript, which was subsequently edited by Greber.

Declaration of competing interest

The authors declare no conflict of interest.

Acknowledgements

The authors thank A. Bekker, I.N. Bindeman, A. Heard, T. Hopp, and T. Meisel for discussions. We thank Hannah Hilbert-Wolf for her assistance in compiling the terrigenous sediment data. Thorough and constructive reviews by J. Korenaga and an anonymous reviewer greatly improved the quality of the manuscript. ND was supported by NASA grants NNX17AE86G (LARS), NNX17AE87G (Emerging Worlds), and 80NSSC17K0744 (Habitable Worlds). NDG was funded by the Swiss National Science Foundation (project number 181172).

Appendix A

For the komatiitic endmember only, we assume that its composition does not change as a function of time. This allows us to estimate the mean value and standard error in each ratio more directly, without having to use the computationally-expensive bootstrap method. However, due to covariance between elements, it is important to consider the ratio as a whole instead of treating the numerator and denominator elements separately. It would also be incorrect to simply compute the mean and standard error of all the ratios, since this would not respect mass balance. The ratio composition of the komatiite endmember, $(A/B)_E$ is not the mean of all the ratios in each individual rock, $(A/B)_i$. Rather, it can be interpreted as a weighted mean, where the weight for each sample is the concentration of the denominator element, $[B]_i$:

$$\left(\frac{A}{B}\right)_E = \frac{\sum_i [A]_i}{\sum_i [B]_i} = \frac{1}{\sum_i [B]_i} \sum_i [B]_i \left(\frac{A}{B}\right)_i$$

Computing the standard error of the weighted mean is a non-trivial matter and has no known closed-form result. We used the variance estimator from Cochran (1977) since its results were found to be the most similar to bootstrap-derived variance by both Gatz and Smith (1995) and our own tests. Using same notation as above, the estimator is of the form:

$$\sigma_E^2 = \frac{N}{(N-1)\left(\sum_i [B]_i\right)^2} \left[\sum_{i=1}^{N} \left([B]_i \left(\frac{A}{B}\right)_i - \overline{[B]} \left(\frac{A}{B}\right)_E \right)^2 - 2\left(\frac{A}{B}\right)_E \sum_{i=1}^{N} \left([B]_i - \overline{[B]}\right) \left([B]_i \left(\frac{A}{B}\right)_i - \overline{[B]} \left(\frac{A}{B}\right)_E \right) + \left(\frac{A}{B}\right)_E^2 \sum_{i=1}^{N} \left([B]_i - \overline{[B]}\right)^2 \right]$$

where the summation i is over all the samples, σ_E^2 is the square of the ratio's standard error in the endmember E, N the number of samples, and $\overline{[B]}$ the average concentration of the denominator element across all samples. Despite the apparent complexity of this equation, its implementation in computer code is much faster to execute than the bootstrap algorithm, which is the reason why it was preferred for the komatiite end-member.

Appendix B

We define q as the total number of elements that can potentially be used and r as the number of ratios that will be used in a reconstruction (for example, $r = 2$ if only the Ni/Co and Th/Sc proxies are used). The total number of possible choices is noted s.

We first consider the situation where an element can only appear once in the set of selected ratios (*e.g.*, [A/B, C/D] is allowed, but [A/B, A/C] is not). As a concrete example, let us consider 6 elements: A, B, C, D, E, and F. There are $\binom{6}{2} = 15$ ways to pair these 6 elements: AB, AC, AD, AE, AF, BC, BD, BE, BF, CD, CE, CF, DE, DF, EF. Once a pairing has been made (*e.g.*, AB), there are $\binom{6-2}{2} = 6$ ways to pair the remaining 6-2=4 elements (CD, CE, CF, DE, DF, EF). If another pairing is added to the set (*e.g.*, CD), there are now $\binom{6-2-2}{2} = 1$ ways to pair the remaining $6-2-2=2$ elements (ED). Enumerating all those possibilities gives a total of

$$\binom{6}{2}\binom{4}{2}\binom{2}{2} = \frac{6!}{2^3} = 90 \quad \text{combinations.}$$

Each chain (*e.g.*, AB-CD-EF) is found in 3! possible arrangements in the enumeration (in this case, these are: AB-CD-EF, AB-EF-CD, CD-AB-EF, CD-EF-AB, EF-AB-CD, EF-CD-AB). The true number of independent combination of ratios that do not involve the repetition of an element is thus

$\frac{6!}{3!2^3} = 15$ combinations.

Enumerating all the possibilities, the 15 allowed combinations in this example are: AB-CD-EF, AB-CE-DF, AB-CF-DE, AC-BD-EF, AC-BE-DF, AC-BF-DE, AD-BC-EF, AD-BE-CF, AD-BF-CE, AE-BC-DF, AE-BD-CF, AE-BF-CD, AF-BC-DE, AF-BD-CE, AF-BE-CD.

In the general case, if one has r pairs to select among $2r$ elements and the elements cannot be repeated in a pair, the number of options will be $(2r)!/(2^r r!)$. There are $\binom{q}{2r}$ manners to select without repetition a set of $2r$ elements out of q elements in total. If an element can only appear once in the set of ratios selected, the total number of permitted combinations is therefore

$$s = \binom{q}{2r}\frac{(2r)!}{2^r r!}.$$

If the same element can appear multiple times in different ratios (*e.g.*, [A/B, A/C] is allowed), many more combinations become possible. There are $\binom{q}{2r}$ ways of selecting without repetition a set of $2r$ elements out of q elements in total. For each such set, there are $\binom{2r}{2}$ possible element pairs and there are $\binom{\binom{2r}{2}}{r}$ ways to pick r ratios out of these $\binom{2r}{2}$ possible pairings. We therefore have

$$s = \binom{q}{2r}\binom{\binom{2r}{2}}{r}.$$

Appendix C. Supplementary material

Supplementary material related to this article can be found online at https://doi.org/10.1016/j.epsl.2020.116090.

References

Arndt, N.T., 2013. The formation and evolution of the continental crust. Geochem. Perspect. 2, 405.

Bas, M.J.L., Streckeisen, A.L., 1991. The IUGS systematics of igneous rocks. J. Geol. Soc. 148, 825–833. https://doi.org/10.1144/gsjgs.148.5.0825.

Bekov, G.I., Letokhov, V.S., Radaev, V.N., Baturin, G.N., Egorov, A.S., Kursky, A.N., Narseyev, V.A., 1984. Ruthenium in the ocean. Nature 312, 748–750. https://doi.org/10.1038/312748a0.

Bindeman, I.N., Zakharov, D.O., Palandri, J., Greber, N.D., Dauphas, N., Retallack, G.J., Hofmann, A., Lackey, J.S., Bekker, A., 2018. Rapid emergence of subaerial landmasses and onset of a modern hydrologic cycle 2.5 billion years ago. Nature 557, 545–548.

Breunig, M.M., Kriegel, H.-P., Ng, R.T., Sander, J., 2000. LOF: identifying density-based local outliers. In: Proceedings of the 2000 ACM SIGMOD International Conference on Management of Data, SIGMOD '00. ACM, New York, NY, USA, pp. 93–104.

Brown, M., Johnson, T., 2018. Secular change in metamorphism and the onset of global plate tectonics. Am. Mineral. 103, 181–196. https://doi.org/10.2138/am-2018-6166.

Cawood, Peter A., Hawkesworth, Chris J., Pisarevsky, Sergei A., Dhuime, Bruno, Capitanio, Fabio A., Oliver, Nebel, 2018. Geological archive of the onset of plate tectonics. Philos. Trans. R. Soc., Math. Phys. Eng. Sci. 376, 20170405. https://doi.org/10.1098/rsta.2017.0405.

Chapman, D.S., 1986. Thermal gradients in the continental crust. Geol. Soc. (Lond.) Spec. Publ. 24, 63–70. https://doi.org/10.1144/GSL.SP.1986.024.01.07.

Chen, K., Rudnick, R.L., Wang, Z., Tang, M., Gaschnig, R.M., Zou, Z., He, T., Hu, Z., Liu, Y., 2019. How mafic was the Archean upper continental crust? Insights from Cu and Ag in ancient glacial diamictites. Geochim. Cosmochim. Acta. https://doi.org/10.1016/j.gca.2019.08.002.

Cochran, W.G., 1977. Sampling Techniques, 3rd edition. Wiley, New-York.

Condie, K.C., 1993. Chemical composition and evolution of the upper continental crust: contrasting results from surface samples and shales. Chem. Geol. 104, 1–37. https://doi.org/10.1016/0009-2541(93)90140-E.

Deng, Z., Chaussidon, M., Guitreau, M., Puchtel, I.S., Dauphas, N., Moynier, F., 2019. An oceanic subduction origin for Archaean granitoids revealed by silicon isotopes. Nat. Geosci. 12, 774–778.

Efron, B., Tibshirani, R., 1986. Bootstrap Methods for Standard Errors, Confidence Intervals, and Other Measures of Statistical Accuracy. Stat. Sci., vol. 1, pp. 54–75.

Flament, N., Coltice, N., Rey, P.F., 2008. A case for late-Archean continental emergence from thermal evolution models and hypsometry. Earth Planet. Sci. Lett. 275, 326–336.

Gaschnig, R.M., Rudnick, R.L., McDonough, W.F., Kaufman, A.J., Valley, J.W., Hu, Z., Gao, S., Beck, M.L., 2016. Compositional evolution of the upper continental crust through time, as constrained by ancient glacial diamictites. Geochim. Cosmochim. Acta 186, 316–343. https://doi.org/10.1016/j.gca.2016.03.020.

Gatz, D.F., Smith, L., 1995. The standard error of a weighted mean concentration—I. Bootstrapping vs other methods. Atmos. Environ. 29, 1185–1193. https://doi.org/10.1016/1352-2310(94)00210-C.

Greber, N.D., Dauphas, N., Bekker, A., Ptáček, M.P., Bindeman, I.N., Hofmann, A., 2017. Titanium isotopic evidence for felsic crust and plate tectonics 3.5 billion years ago. Science 357, 1271–1274. https://doi.org/10.1126/science.aan8086.

Greber, N.D., Dauphas, N., 2019. The chemistry of fine-grained terrigenous sediments reveals a chemically evolved paleoarchean emerged crust. Geochim. Cosmochim. Acta 255, 247–264.

Herzberg, C., Condie, K., Korenaga, J., 2010. Thermal history of the Earth and its petrological expression. Earth Planet. Sci. Lett. 292, 79–88.

Holder, R.M., Viete, D.R., Brown, M., Johnson, T.E., 2019. Metamorphism and the evolution of plate tectonics. Nature. https://doi.org/10.1038/s41586-019-1462-2.

Hopkins, M., Harrison, T.M., Manning, C.E., 2008. Low heat flow inferred from >4 Gyr zircons suggests Hadean plate boundary interactions. Nature 456, 493–496. https://doi.org/10.1038/nature07465.

Jaupart, C., Labrosse, S., Lucazeau, F., Mareschal, J.-C., 2015. 7.06 - temperatures, heat, and energy in the mantle of the Earth. In: Schubert, G. (Ed.), Treatise on Geophysics, second edition. Elsevier, Oxford, pp. 223–270.

Keller, C.B., Schoene, B., 2012. Statistical geochemistry reveals disruption in secular lithospheric evolution about 2.5Gyr ago. Nature 485, 490–493. https://doi.org/10.1038/nature11024.

Keller, B., Schoene, B., 2018. Plate tectonics and continental basaltic geochemistry throughout Earth history. Earth Planet. Sci. Lett. 481, 290–304. https://doi.org/10.1016/j.epsl.2017.10.031.

Korenaga, J., 2013. Initiation and evolution of plate tectonics on Earth: theories and observations. Annu. Rev. Earth Planet. Sci. 41, 117–151. https://doi.org/10.1146/annurev-earth-050212-124208.

Korenaga, J., Planavsky, N.J., Evans, D.A.D., 2017. Global water cycle and the coevolution of the Earth's interior and surface environments. Philos. Trans. R. Soc. A 375, 20150393.

Kriegel, H.-P., Kröger, P., Schubert, E., Zimek, A., 2009. LoOP: local outlier probabilities. In: Proceedings of the 18th ACM Conference on Information and Knowledge Management, CIKM '09. ACM, New York, NY, USA, pp. 1649–1652.

Lange, O.F., Grubmüller, H., 2006. Generalized correlation for biomolecular dynamics. Proteins 62, 1053–1061.

Large, R.R., Mukherjee, I., Zhukova, I., Corkrey, R., Stepanov, A., Danyushevsky, L.V., 2018. Role of upper-most crustal composition in the evolution of the Precambrian ocean–atmosphere system. Earth Planet. Sci. Lett. 487, 44–53. https://doi.org/10.1016/j.epsl.2018.01.019.

McDonough, W.F., Sun, S.-s., 1995. The composition of the Earth. Chem. Geol. 120, 223–253. https://doi.org/10.1016/0009-2541(94)00140-4.

Metropolis, N., Rosenbluth, A.W., Rosenbluth, M.N., Teller, A.H., Teller, E., 1953. Equation of state calculations by fast computing machines. J. Chem. Phys. 21, 1087–1092. https://doi.org/10.1063/1.1699114.

Moyen, J.-F., Martin, H., 2012. Forty Years of TTG Research. Lithos, vol. 148, pp. 312–336.

Nozaki, Y., 1997. A fresh look at element distribution in the North Pacific Ocean. Eos Trans. AGU 78, 221. https://doi.org/10.1029/97EO00148.

Roman, A., Arndt, N., 2019. Differentiated Archean oceanic crust: Its thermal structure, mechanical stability and a test of the sagduction hypothesis. Geochim. Cosmochim. Acta. https://doi.org/10.1016/j.gca.2019.07.009.

Rosas, J.C., Korenaga, J., 2018. Rapid crustal growth and efficient crustal recycling in the early Earth: implications for Hadean and Archean geodynamics. Earth Planet. Sci. Lett. 494, 42–49.

Rudnick, R.L., Gao, S., 2003. Composition of the continental crust (3.01). In: Turekian, K.K. (Ed.), Treatise on Geochemistry. Pergamon, Oxford, pp. 1–64.

Rudnick, R.L., McDonough, W.F., O'Connell, R.J., 1998. Thermal structure, thickness and composition of continental lithosphere. Chem. Geol. 145, 395–411. https://doi.org/10.1016/S0009-2541(97)00151-4.

Schubert, E., Zimek, A., Kriegel, H.-P., 2014. Local outlier detection reconsidered: a generalized view on locality with applications to spatial, video, and network outlier detection. Data Min. Knowl. Discov. 28, 190–237. https://doi.org/10.1007/s10618-012-0300-z.

Smit, M.A., Mezger, K., 2017. Earth's early O2 cycle suppressed by primitive continents. Nat. Geosci. https://doi.org/10.1038/ngeo3030. Advance online publication.

Smithies, R.H., 2000. The Archaean tonalite–trondhjemite–granodiorite (TTG) series is not an analogue of Cenozoic adakite. Earth Planet. Sci. Lett. 182, 115–125. https://doi.org/10.1016/S0012-821X(00)00236-3.

Sohrin, Y., Fujishima, Y., Ueda, K., Akiyama, S., Mori, K., Hasegawa, H., Matsui, M., 1998. Dissolved niobium and tantalum in the North Pacific. Geophys. Res. Lett. 25, 999–1002. https://doi.org/10.1029/98GL00646.

Sun, W., 2018. The formation of the continental crust. Solid Earth Sci. 3, 31–32. https://doi.org/10.1016/j.sesci.2018.03.003.

Tang, M., Chen, K., Rudnick, R.L., 2016. Archean upper crust transition from mafic to felsic marks the onset of plate tectonics. Science 351, 372–375. https://doi.org/10.1126/science.aad55133.

Taylor, S.R., McLennan, S.M., 1985. The Continental Crust: Its Composition and Evolution.

Wedepohl, H.K., 1995. The composition of the continental crust. Geochim. Cosmochim. Acta 59, 1217–1232. https://doi.org/10.1016/0016-7037(95)00038-2.